Time-stepping and Krylov methods for large-scale instability problems

J.-Ch. Loiseau, M. A. Bucci, and J.-Ch. Robinet

Abstract ???

1 Introduction

2 Theoretical framework

Our attention is focused on the characterization of very high-dimensional nonlinear dynamical systems typically arising from the spatial discretization of partial differential equations such as the incompressible Navier-Stokes equations. In general, the resulting dynamical equations are written down as a system of first order differential equations

$$\dot{X}_j = \mathcal{F}_j\left(\{X_i(t);\ i = 1,\cdots,n\},t\right)$$

where the integer n is the *dimension* of the system, and $\dot{X}_j$ denotes the time-derivative of X_j. Using the notation $\mathbf{X}$ and $\boldsymbol{\mathcal{F}}$ for the sets $\left\{X_j,\ i = 1,\cdots,n\right\}$ and $\left\{\mathcal{F}_j,\ i = 1,\cdots,n\right\}$, this system can be compactly written as

$$\dot{\mathbf{X}} = \boldsymbol{\mathcal{F}}(\mathbf{X},t), \tag{1}$$

J.-Ch. Loiseau
Laboratoire DynFluid, Arts et Métiers ParisTech, 151 boulevard de l'hôpital, 75013 Paris, France.
e-mail: jean-christophe.loiseau@ensam.eu

M. A. Bucci
Laboratoire DynFluid, Arts et Métiers ParisTech, 151 boulevard de l'hôpital, 75013 Paris, France.
e-mail: michele.bucci@ensam.eu

J.-Ch. Robinet
Laboratoire DynFluid, Arts et Métiers ParisTech, 151 boulevard de l'hôpital, 75013 Paris, France.
e-mail: jean-christophe.robinet@ensam.eu

where $\mathbf{X}$ is the $n \times 1$ *state vector* of the system and t is a continuous variable denoting time. Alternatively, accounting also for temporal discretization gives rise to a discrete-time dynamical system

$$X_{j,k+1} = \mathcal{G}_j\left(\left\{X_{i,k};\ i = 1, \cdots, n\right\}, k\right)$$

or formally

$$\mathbf{X}_{k+1} = \boldsymbol{\mathcal{G}}\left(\mathbf{X}_k, k\right) \tag{2}$$

where the index k now denotes the discrete time variable. If one uses first-order Euler extrapolation for the time discretization, the relation between $\boldsymbol{\mathcal{F}}$ and $\boldsymbol{\mathcal{G}}$ is given by

$$\boldsymbol{\mathcal{G}}(\mathbf{X}) = \mathbf{X} + \Delta t \boldsymbol{\mathcal{F}}(\mathbf{X}),$$

where Δt is the time-step and the explicit dependences on t and k have been dropped for the sake of simplicity.

In the rest of this section, the reader will be introduced to the concepts of fixed points and linear stability, two concepts required to characterize a number of properties of the system investigated. Particular attention will be paid to *modal* and *nonmodal stability*, two approaches that have become increasingly popular in fluid dynamics over the past decades. Note that the concept of *nonlinear optimal perturbation*, which has raised a lot attention lately, is beyond the scope of the present contribution. For interested readers, please refer to the recent work by [7] and references therein.

Finally, while we will mostly use the continuous-time representation (1) when introducing the reader to the theoretical concepts exposed in this section, using the discrete-time representation (2) will prove more useful when discussing and implementing the different algorithms presented in §3.

2.1 Fixed points

Nonlinear dynamical systems described by Eq. (1) or Eq. (2) tend to admit a number of different equilibria forming the backbone of their phase space. These different equilibria can take the form of fixed points, periodic orbits, torus or strange attractors for instance. In the rest of this work, our attention will be solely focused on fixed points.

For a continuous-time dynamical system described by Eq. (1), fixed points $\mathbf{X}^*$ are solution to

$$\boldsymbol{\mathcal{F}}(\mathbf{X}) = 0. \tag{3}$$

Conversely, fixed points $\mathbf{X}^*$ of a discrete-time dynamical system described by Eq. (2) are solution to

$$\boldsymbol{\mathcal{G}}(\mathbf{X}) = \mathbf{X}. \tag{4}$$

It must be emphasized that both Eq. (3) and Eq. (4) may admit multiple solutions. Such a multiplicity of fixed points can easily be illustrated by a dynamical system as simple as the following Duffing oscillator

$$\begin{aligned} \dot{x} &= y \\ \dot{y} &= -\frac{1}{2}y + x - x^3. \end{aligned} \tag{5}$$

Despite its apparent simplicity, this Duffing oscillator admits three fixed points, namely

- a saddle at the origin $\mathbf{X}^* = (0,0)$,
- two linearly stable spirals located at $\mathbf{X}^* = (\pm 1, 0)$.

All of these fixed points, along with some trajectories, are depicted on figure 1 for the sake of illustration. Such a multiplicity of fixed points also occurs in dynamical systems as complex as the Navier-Stokes equations. Determining which of these fixed points is the most relevant one from a physical point of view is problem-dependent and left for the user to decide. Note however that computing these equilibrium points is a prerequisite to all of the analyses to be described in this chapter. Numerical methods to solve Eq. (3) or Eq. (4) will be discussed in §3.1.

2.2 Linear stability analysis

Having computed a given fixed point $\mathbf{X}^*$ of a continuous-time nonlinear dynamical system given by Eq. (1), one may ask whether it corresponds to a stable or unstable equilibrium of the system. Before pursuing, the very notion of *stability* needs to be explained. It is traditionally defined following the concept of Lyapunov stability. Having computed the equilibrium state $\mathbf{X}^*$, the system is perturbed around this state. If it returns back to the equilibrium point, the latter is deemed stable, otherwise, it

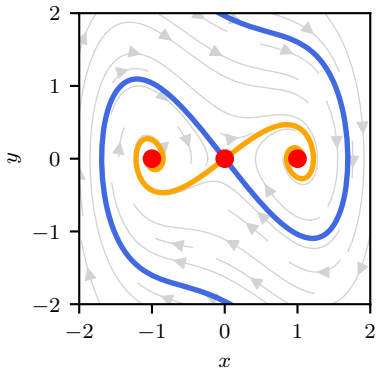

Fig. 1 Phase portrait of the unforced Duffing oscillator (5). The red dots denote the three fixed points admitted by the system. The blue (resp. orange) thick line depicts the stable (resp. unstable) manifold of the saddle point located at the origin. Grey lines highlight a few trajectories exhibited for different initial conditions.

is regarded as unstable. It has to be noted that, in the concept of Lyapunov stability, an infinite time horizon is allowed for the return to equilibrium.

The dynamics of a perturbation $\mathbf{x} = \mathbf{X} - \mathbf{X}^*$ are governed by

$$\dot{\mathbf{x}} = \boldsymbol{\mathcal{F}}(\mathbf{X}^* + \mathbf{x}). \tag{6}$$

Assuming the perturbation $\mathbf{x}$ is infinitesimal, $\boldsymbol{\mathcal{F}}(\mathbf{X})$ can be approximated by its first-order Taylor expansion around $\mathbf{X} = \mathbf{X}^*$. Doing so, the governing equations for the perturbation $\mathbf{x}$ simplify to

$$\dot{\mathbf{x}} = \boldsymbol{\mathcal{A}}\mathbf{x}, \tag{7}$$

where $\boldsymbol{\mathcal{A}}$ is the $n \times n$ Jacobian matrix of $\boldsymbol{\mathcal{F}}$. Starting from an initial condition $\mathbf{x}_0$, the perturbation at time t is given by

$$\mathbf{x}(t) = \exp(\boldsymbol{\mathcal{A}}t)\,\mathbf{x}_0. \tag{8}$$

The operator $\boldsymbol{\mathcal{M}}(t) = \exp(\boldsymbol{\mathcal{A}}t)$ is known as the *exponential propagator*. Introducing the spectral decomposition of $\boldsymbol{\mathcal{A}}$

$$\boldsymbol{\mathcal{A}} = \boldsymbol{\mathcal{V}}\boldsymbol{\Lambda}\boldsymbol{\mathcal{V}}^{-1},$$

Eq. (8) can be rewritten as

$$\mathbf{x}(t) = \boldsymbol{\mathcal{V}}\exp(\boldsymbol{\Lambda}t)\,\boldsymbol{\mathcal{V}}^{-1}\mathbf{x}_0, \tag{9}$$

where the i$^{\text{th}}$ column of $\boldsymbol{\mathcal{V}}$ is the eigenvector $\mathbf{v}_i$ associated to the i$^{\text{th}}$ eigenvalue $\lambda_i = \boldsymbol{\Lambda}_{ii}$, with $\boldsymbol{\Lambda}$ a diagonal matrix. Assuming that the eigenvalues of $\boldsymbol{\mathcal{A}}$ have been sorted by decreasing real part, it can easily be shown that

$$\lim_{t\to+\infty} \exp(\boldsymbol{\mathcal{A}}t)\,\mathbf{x}_0 = \lim_{t\to+\infty} \exp(\lambda_1 t)\,\mathbf{v}_1.$$

The asymptotic fate of an initial perturbation $\mathbf{x}_0$ is thus entirely dictated by the real part of the leading eigenvalue λ_1:

- if $\Re(\lambda_1) > 0$, a random initial perturbation $\mathbf{x}_0$ will eventually grow exponentially rapidly. Hence, the fixed point $\mathbf{X}^*$ is deemed *linearly unstable*.
- If $\Re(\lambda_1) < 0$, the initial perturbation $\mathbf{x}_0$ will eventually decay exponentially rapidly. The fixed point $\mathbf{X}^*$ is thus *linearly stable*.

The case $\Re(\lambda_1) = 0$ is peculiar. The fixed point $\mathbf{X}^*$ is called *elliptic* and one cannot conclude about its stability solely by looking at the eigenvalues of $\boldsymbol{\mathcal{A}}$. In this case, one needs to resort to *weakly non-linear analysis* which essentially looks at the properties of higher-order Taylor expansion of $\boldsymbol{\mathcal{F}}(\mathbf{X})$. Once again, this is beyond the scope of the present chapter. Interested readers are referred to [**?**] for more details about such analyses.

Illustration

Let us illustrate the notion of linear stability on a simple example. For that purpose, we will consider the same linear dynamical system as in [13]. This system reads

$$\frac{\mathrm{d}}{\mathrm{d}t}\begin{bmatrix} x_1 \\ x_2 \end{bmatrix} = \underbrace{\begin{bmatrix} \frac{1}{100} - \frac{1}{Re} & 0 \\ 1 & -\frac{2}{Re} \end{bmatrix}}_{\boldsymbol{\mathcal{A}}} \begin{bmatrix} x_1 \\ x_2 \end{bmatrix} \tag{10}$$

where Re is a control parameter. For such a simple case, it is obvious that the eigenvalues of $\boldsymbol{\mathcal{A}}$ are given by

$$\lambda_1 = \frac{1}{100} - \frac{1}{Re}$$

and

$$\lambda_2 = -\frac{2}{Re}.$$

While λ_2 is constantly negative, λ_1 is negative for $Re < 100$ and positive otherwise. Figure 2 depicts the time-evolution of $\|\mathbf{x}\|_2^2 = x_1^2 + x_2^2$ for two different values of Re. Please note that the short-time ($t < 100$) behavior of the perturbation will be discussed in §2.3. It is clear nonetheless that, for $t > 100$, the time-evolution of the perturbation can be described by an exponential function. Whether this exponential increases or decreases as a function of time is solely dictated by the sign of λ_1, negative for $Re = 50$ and positive for $Re = 100$. For $Re = 50$, the equilibrium point $\mathbf{X}^* = \begin{bmatrix} 0 & 0 \end{bmatrix}^T$ is thus stable, while it is unstable for $Re = 125$.

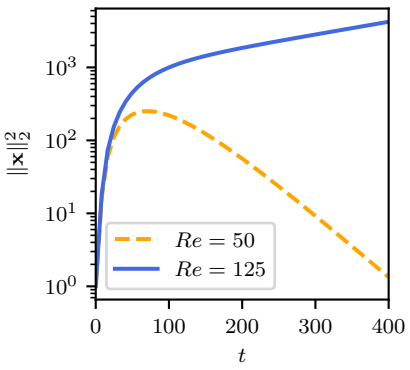

Fig. 2 Evolution as a function of time of $\|\mathbf{x}\|_2^2 = x_1^2 + x_2^2$ for the toy-model (10). For $Re = 50$ (resp. $Re = 125$), the asymptotic fate of $\|\mathbf{x}\|_2^2$ is described by a decreasing (resp. increasing) exponential. For $Re = 50$, the equilibrium point is thus linear stable, while it is linearly unstable for $Re = 125$.

2.3 Non-modal stability analysis

Looking once more at figure 2, it can be seen that, although the system is linearly stable for $Re = 50$, the perturbation $\mathbf{x}$ can experience a transient growth of its energy for a short period of time, roughly given by $0 < t < 100$ in the present case, before its eventual exponential decay. This behavior is related to the *non-normality* of $\boldsymbol{\mathcal{A}}$, i.e.

$$\boldsymbol{\mathcal{A}}^\dagger \boldsymbol{\mathcal{A}} \neq \boldsymbol{\mathcal{A}} \boldsymbol{\mathcal{A}}^\dagger, \tag{11}$$

where $\boldsymbol{\mathcal{A}}^\dagger$ is the *adjoint* of $\boldsymbol{\mathcal{A}}$. As a result of this non-normality, the eigenvectors of $\boldsymbol{\mathcal{A}}$ do not form an orthonormal set of vectors[1]. The consequences of this non-orthogonality of the set of eigenvectors can be visualized on figure 3 where the trajectory stemming from a random unit-norm initial condition $\mathbf{x}_0$ is depicted in the phase plane of our toy-model (10). The perturbation $\mathbf{x}(t)$ is first attracted toward the linear manifold associated to the least stable eigenvalue λ_1, causing in the process the transient growth of its energy by a factor 300. Once it reaches the vicinity of the linearly stable manifold, the perturbation eventually decays exponentially rapidly along this eigendirection of the fixed point. The next sections are devoted to the introduction of mathematical tools particularly useful to characterize phenomena resulting from this non-normality of $\boldsymbol{\mathcal{A}}$, both in the time and frequency domains, when the fixed point considered is stable.

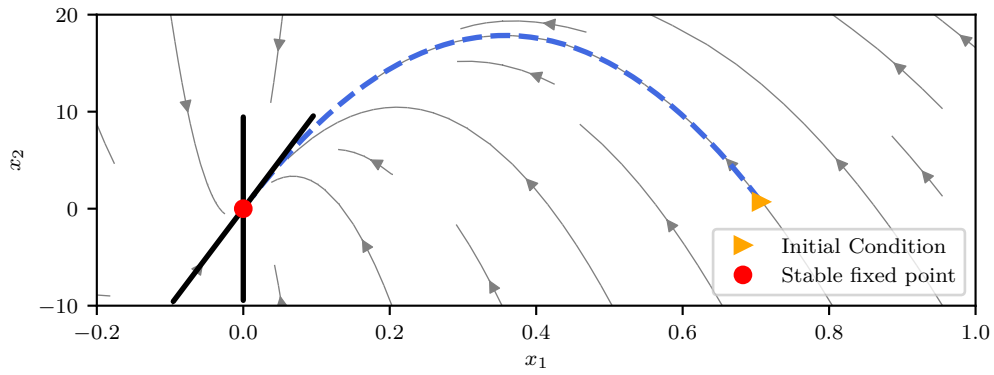

Fig. 3 The blue (dashed) line shows the trajectory stemming from a random unit-norm initial condition $\mathbf{x}_0$. The thick black lines depict the two linear manifolds of the fixed point. The diagonal one corresponds to $\lambda_1 = 1/100 - 1/Re$, while the vertical one is associated to $\lambda_2 = -2/Re$. In the present case, Re is set to 50, thus corresponding to a situation where the fixed point is linearly stable. Note that different scales are used for the horizontal and vertical axes.

[1] Note that the non-normality of $\boldsymbol{\mathcal{A}}$ also implies that its right and left eigenvectors are different. As will be discussed in §4, this observation may have large consequences in fluid dynamics, particularly when addressing the problems of optimal linear control and/or estimation of strongly non-parallel flows.

2.3.1 Optimal perturbation analysis

Having observed that a random initial condition can experience a relatively large transient growth of its energy over a short period of time even though the fixed point is stable, one may be interested in the worst case scenario, i.e. finding which initial condition $\mathbf{x}_0$ is amplified as much as possible before it eventually decays. Searching for such a perturbation is known as *optimal perturbation analysis* and can be addressed by two different methods:

- Optimization,
- Singular Value Decomposition (SVD).

Both approaches will be presented. Although it requires the introduction of additional mathematical concepts, the approach relying on optimization will be introduced first in §2.3.1 as it easier to grasp. The approach relying on singular value decomposition of the exponential propagrator $\boldsymbol{\mathcal{M}} = \exp(\boldsymbol{\mathcal{A}}t)$ will then be presented in §2.3.1.

Formulation as an optimization problem

The aim of optimal perturbation analysis is to find the unit-norm initial condition $\mathbf{x}_0$ that maximizes $\|\mathbf{x}(T)\|_2^2$, where T is known as the *target time*. Note that we here consider only the 2-norm of $\mathbf{x}(T)$ for the sake of simplicity, although one could formally optimize different norms, see [**?**] for examples from fluid dynamics. For a given target time T, such a problem can be formulated as the following constrained maximization problem

$$\begin{aligned} &\underset{\mathbf{x}_0}{\text{maximize}}\ \mathcal{J}(\mathbf{x}_0) = \|\mathbf{x}(T)\|_2^2 \\ &\text{subject to } \dot{\mathbf{x}} - \boldsymbol{\mathcal{A}}\mathbf{x} = 0 \\ &\qquad\qquad \|\mathbf{x}_0\|_2^2 - 1 = 0, \end{aligned} \tag{12}$$

where $\mathcal{J}(\mathbf{x}_0)$ is known as the *objective function*. It must be emphasized that problem (12) is not formulated as a convex optimization problem[2]. As such, it may exhibit local maxima. Nonetheless, this constrained maximization problem can be recast into the following unconstrained maximization problem

[2] Formally, a convex optimization problem reads

$$\begin{aligned} &\underset{\mathbf{x}}{\text{minimize}}\ \mathcal{J}(\mathbf{x}) \\ &\text{subject to } g_i(\mathbf{x}) \leq 0,\ i = 1, \cdots, m \\ &\qquad\qquad h_i(\mathbf{x}) = 0,\ i = 1, \cdots, p, \end{aligned}$$

where the objective function $\mathcal{J}(\mathbf{x})$ and the inequality constraints functions $g_i(\mathbf{x})$ are convex. The conditions on the equality constraints functions $h_i(\mathbf{x})$ are more restrictive as they need to be affine functions, i.e. of the form $h_i(\mathbf{x}) = \mathbf{a}_i^T\mathbf{x} + b_i$. See the book by Boyd & Vandenberghe [2] for extensive details about convex optimization.

$$\underset{\mathbf{x},\mathbf{v},\mu}{\text{maximize}}\ \mathcal{L}(\mathbf{x},\mathbf{v},\mu), \tag{13}$$

where

$$\mathcal{L}(\mathbf{x},\mathbf{v},\mu) = \mathcal{J}(\mathbf{x}_0) + \int_0^T \mathbf{v}^T(\dot{\mathbf{x}} - \boldsymbol{\mathcal{A}}\mathbf{x})\,\mathrm{d}t + \mu\left(\|\mathbf{x}_0\|_2^2 - 1\right) \tag{14}$$

is known as the *augmented Lagrangian* function. The additional optimization variables $\mathbf{v}$ and μ appearing in the definition of the augmented Lagrangian $\mathcal{L}$ are called *Lagrange multipliers*. Solutions to problem (13) are identified by vanishing first variations of $\mathcal{L}$ with respect to our three optimization variables. The first variation of $\mathcal{L}$ with respect to $\mathbf{v}$ and μ are simply the constraints of our original problem (12). The first variation of $\mathcal{L}$ with respect to $\mathbf{x}$ on the other hand is given by

$$\delta_{\mathbf{x}}\mathcal{L} = [\nabla_{\mathbf{x}}\mathcal{J} + \mathbf{v}(T)]\cdot\delta\mathbf{x}(0) + \int_0^T \left[\dot{\mathbf{v}} - \boldsymbol{\mathcal{A}}^\dagger\mathbf{v}\right]\cdot\delta\mathbf{x}\,\mathrm{dt} + [2\mu\mathbf{x}_0 - \mathbf{v}(0)]\cdot\delta\mathbf{x}(0). \tag{15}$$

Eq. (15) vanishes only if

$$\dot{\mathbf{v}} = \boldsymbol{\mathcal{A}}^\dagger\mathbf{v} \ \text{ over } t\in(0,T), \tag{16}$$

and

$$\begin{aligned} \nabla_{\mathbf{x}}\mathcal{J} - \mathbf{v}(T) &= 0 \\ 2\mu\mathbf{x}_0 - \mathbf{v}(0) &= 0. \end{aligned} \tag{17}$$

Note that Eq. (16) is known as the adjoint system[3] of our original linear dynamical system, while Eq. (17) are called compatibility conditions. Maximizing $\mathcal{L}$ is then a problem of simultaneously satisfying (7), (16) and (17). This is in general done iteratively by gradient-based algorithms such as gradient ascent or the rotation-update gradient algorithm (see §3). For more details about adjoint-based optimization, see [2, 7].

Formulation using SVD

As stated previously, formulating the optimal perturbation analysis as a constrained maximization results in a non-convex optimization problem (12). Consequently, although a solution to (12) can easily be obtained by means of gradient-based algo-

[3] Given an appropriate inner product, the adjoint operator $\boldsymbol{\mathcal{A}}^\dagger$ is defined such that

$$\langle\mathbf{v}|\boldsymbol{\mathcal{A}}\mathbf{x}\rangle = \langle\boldsymbol{\mathcal{A}}^\dagger\mathbf{v}|\mathbf{x}\rangle,$$

where $\langle\mathbf{a}|\mathbf{b}\rangle$ denotes the inner product of $\mathbf{a}$ and $\mathbf{b}$. If one consider the classical Euclidean inner product, the adjoint operator is simply given by

$$\boldsymbol{\mathcal{A}}^\dagger = \boldsymbol{\mathcal{A}}^H$$

where $\boldsymbol{\mathcal{A}}^H$ is the Hermitian (i.e. complex-conjugate transpose) of $\boldsymbol{\mathcal{A}}$. It must be noted finally that the direct operator $\boldsymbol{\mathcal{A}}$ and the adjoint one $\boldsymbol{\mathcal{A}}^\dagger$ have the same eigenspectrum. This last observation is a key point when one aims at validating the numerical implementation of an adjoint solver.

rithms, one cannot rule out the possibility that this solution is only a local maxima rather than the global one. In this section, we will show that recasting problem (12) in the framework of linear algebra however allows us to obtain easily this global optimal.

Let us first redefine our optimization problem as

$$\underset{\mathbf{x}_0}{\text{maximize}} \ \frac{\|\mathbf{x}(T)\|_2^2}{\|\mathbf{x}_0\|_2^2} \tag{18}$$

so that rather than maximizing $\|\mathbf{x}(T)\|_2^2$ under the constraint that $\|\mathbf{x}_0\|_2^2 = 1$, we now directly aim to maximize the energy gain $\mathcal{G}(T) = {}^{\|\mathbf{x}(T)\|_2^2}/_{\|\mathbf{x}_0\|_2^2}$. Moreover, recalling from (8) that

$$\mathbf{x}(T) = \exp(\boldsymbol{\mathcal{A}}T)\,\mathbf{x}_0,$$

our energy gain maximization problem can finally be written as

$$\begin{aligned} \mathcal{G}(T) &= \max_{\mathbf{x}_0} \frac{\|\exp(\boldsymbol{\mathcal{A}}t)\,\mathbf{x}_0\|_2^2}{\|\mathbf{x}_0\|_2^2} \\ &= \|\exp(\boldsymbol{\mathcal{A}}T)\|_2^2 \end{aligned} \tag{19}$$

where $\|\exp(\boldsymbol{\mathcal{A}}T)\|_2$ is a vector-induced matrix norm taking care of the optimization over all possible initial conditions $\mathbf{x}_0$. Introducing singular value decomposition (SVD), i.e.

$$\boldsymbol{\mathcal{M}} = \boldsymbol{\mathcal{U}}\boldsymbol{\Sigma}\boldsymbol{\mathcal{V}}^H,$$

it is relatively easy to demonstrate that the optimal energy gain $\mathcal{G}(T)$ is given by

$$\mathcal{G}(T) = \sigma_1^2, \tag{20}$$

where σ_1 is the largest singular value of the exponential propagator $\boldsymbol{\mathcal{M}} = \exp(\boldsymbol{\mathcal{A}}T)$. The optimal initial condition $\mathbf{x}_0$ is then given by the principal right singular vector (i.e. $\mathbf{x}_0 = \mathbf{v}_1$), while the associated response is given by $\mathbf{x}(T) = \sigma_1\mathbf{u}_1$, where $\mathbf{u}_1$ is the principal left singular vector.

Illustration

As to illustrate linear optimal perturbations, let us consider the incompressible flow of a Newtonian fluid induced by two flat plates moving in-plane in opposite directions as sketched on figure 4(a). The resulting flow, known as *plane Couette flow*, is given by

$$U(y) = y.$$

Note that it is a linearly stable fixed point of the Navier-Stokes equations no matter the Reynolds number considered. Despite its linear stability, subcritical transition to turbulence can occur for Reynolds numbers as low as $Re = ??$.

Without getting to deep into the mathematical and physical details of such subcritical transition, part of the explanation can be given by linear optimal perturbation analysis. The dynamics of an infinitesimal perturbation $\mathbf{x} = \begin{bmatrix}\mathbf{v} & \eta\end{bmatrix}^T$, characterized by a certain wavenumber $\mathbf{k} = \alpha\mathbf{e}_x + \beta\mathbf{e}_z$, evolving in the vicinity of this fixed point are governed by

$$\frac{\mathrm{d}}{\mathrm{d}t}\begin{bmatrix}\mathbf{v}\\ \eta\end{bmatrix} = \begin{bmatrix}\mathcal{A}_{OS} & 0\\ \mathcal{C} & \mathcal{A}_S\end{bmatrix}\begin{bmatrix}\mathbf{v}\\ \eta\end{bmatrix} \tag{21}$$

where $\mathbf{v}$ is the wall-normal velocity of the perturbation and η its wall-normal vorticity, $\mathcal{A}_{OS}$ is the Orr-Sommerfeld operator, while $\mathcal{A}_S$ is the Squire one. The operator $\mathcal{C}$ describes the existing coupling between the wall-normal velocity $\mathbf{v}$ and the wall-normal vorticity η. For certain pairs of wavenumbers, this Orr-Sommerfeld-Squire operator is highly non-normal and perturbations can exhibit very large transient growth. This is illustrated on figure 4(a) where the evolution of the optimal gain $\mathcal{G}(T)$ as a function of the target time T is depicted for different pairs of wavenumbers (α,β). The maximum amplification achievable over all target times T and wavenumbers pairs (α,β) is $\mathcal{G}_{\text{opt}} \simeq 100$. The initial perturbation $\mathbf{x}_0$ corresponding to this optimal energy gain is depicted on figure 4(b). It corresponds to streamwise-oriented vortices that eventually give rise to streamwise velocity streaks due to the lift-up effect [9, 3], see figure 4(d). While this perturbation eventually decays exponentially rapidly in a purely linear framework, it has been shown that, for a sufficiently large initial amplitude, it may eventually trigger transition to turbulence when used as initial condition in a non-linear direct numerical simulation of the Navier-Stokes equations [**?**]. For more details about subcritical transition and extension of optimal perturbation analysis to non-linear operators, interested readers are referred to [**?**].

2.3.2 Resolvent analysis

The optimal perturbation analysis (see §2.3.1) aims at finding the initial condition $\mathbf{x}_0$ that maximizes the transient amplification of energy of the response $\mathbf{x}(T) = \exp(\mathcal{A}T)\,\mathbf{x}_0$ at the target time $t = T$. It is thus an initial-value problem that can be investigated in the time domain. Rather than considering the response of the system to different initial conditions, one may instead wonder how the system reacts to external noise. For that purpose, let us now consider a forced linear dynamical system

$$\dot{\mathbf{x}} = \mathcal{A}\mathbf{x} + \mathbf{f} \tag{22}$$

where the forcing $\mathbf{f}$ now models the system's input such as the external noise. As before, we moreover assume that all of the eigenvalues of $\mathcal{A}$ lie within the stable half of the complex plane. As for the optimal perturbation analysis, one may now consider a worst-case scenario, i.e. what is the forcing $\mathbf{f}$ that maximizes the asymptotic response of the system? Because we consider a linear dynamical system, this question can naturally be addressed in the frequency domain.

In the most general case, the response of the system to the forcing $\mathbf{f}(t)$ is given by

$$\mathbf{x}(t) = \int_0^t \exp\left(\boldsymbol{\mathcal{A}}(t-\tau)\right)\mathbf{f}(\tau)\,\mathrm{d}\tau \tag{23}$$

which is a convolution integral. Note that, in the above expression, we assumed a zero initial condition, i.e. $\mathbf{x}_0 = 0$. Such a convolution integral is also known as a memory integral and highlights that the current state $\mathbf{x}(t)$ of the system depends on the entire history of the forcing $\mathbf{f}$. Because we consider linear stable systems, the influence of the forcing on the current state decays exponentially according to the least stable eigenvalue. Let us assume furthermore a harmonic external forcing

$$\mathbf{f}(t) = \Re\left(\hat{\mathbf{f}}e^{i\omega t}\right) \tag{24}$$

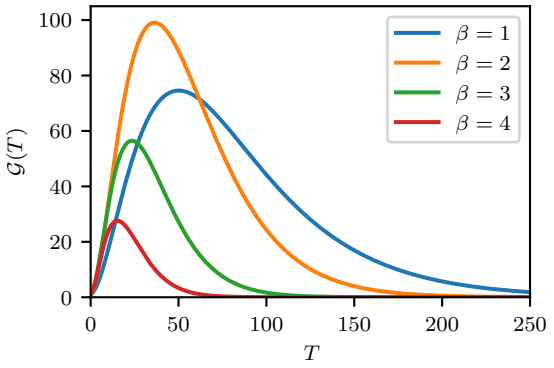

(a)

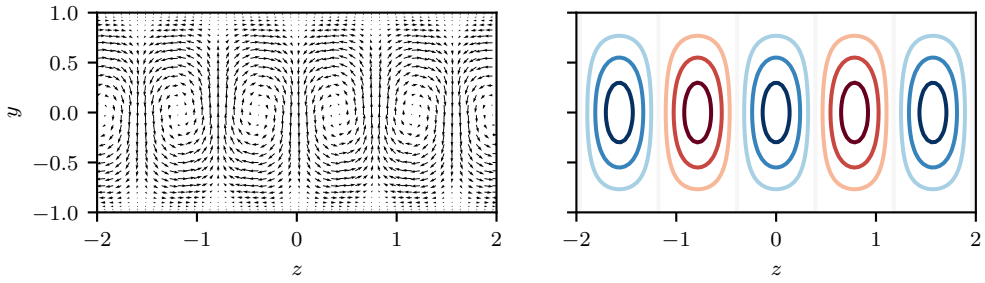

(b)

Fig. 4 Illustration of optimal perturbation analysis for the plane Couette flow at $Re = 300$. In all cases, the streamwise wavenumber of the perturbation is set to $\alpha = 0$. (a) Optimal gain curve for different spanwise wavenumbers β. (b) Optimal perturbation (left) and optimal response (right) for $\beta = 2$. Note that optimal perturbation consists of streamwise oriented vortices, while the associated response at time T consist in high- and low-speed streaks.

where $\omega \in \mathbb{R}$ is the circular frequency of the forcing. The convolution integral can now be easily computed in the frequency domain. Given our assumptions, the asymptotic response of the system at the frequency ω is given by

$$\hat{\mathbf{x}} = (i\omega\mathcal{I} - \boldsymbol{\mathcal{A}})^{-1}\hat{\mathbf{f}}. \tag{25}$$

The operator $\boldsymbol{\mathcal{R}}(\omega) = (i\omega\mathcal{I} - \boldsymbol{\mathcal{A}})^{-1}$ appearing in Eq. (25) is known as the *Resolvent operator* and is related to the exponential propagator $\boldsymbol{\mathcal{M}}(t) = \exp(\boldsymbol{\mathcal{A}}t)$ via Laplace transform. This operator, acting in the frequency domain, maps the input harmonic forcing $\hat{\mathbf{f}}(\omega)$ to the output harmonic response $\hat{\mathbf{x}}(\omega)$.

Finding the forcing frequency ω that maximizes the asymptotic response $\mathbf{x}$ of the system can now be formalized as

$$\begin{aligned}\mathcal{R}(\omega) &= \max_{\hat{\mathbf{f}}} \frac{\| (i\omega\mathcal{I} - \boldsymbol{\mathcal{A}})^{-1}\hat{\mathbf{f}}\|_2^2}{\|\hat{\mathbf{f}}\|_2^2} \\ &= \|\boldsymbol{\mathcal{R}}(\omega)\|_2^2.\end{aligned} \tag{26}$$

Going from the time domain to the frequency domain, the norm of the exponential propagator is replaced with that of the resolvent in order quantify the energy amplification between the input forcing and the output response. As before, the optimal resolvent gain at the frequency ω is given by

$$\mathcal{R}(\omega) = \sigma_1^2,$$

where σ_1 is the largest singular value of $\boldsymbol{\mathcal{R}}(\omega)$. The associated optimal forcing $\hat{\mathbf{f}}$ and response $\hat{\mathbf{x}}$ are then given by the corresponding right and left singular vectors, respectively.

Illustration

Once more, let us illustrate the use of the resolvent analysis on an example from fluid dynamics. For that purpose, we will consider an axisymmetric jet whose radial velocity profile is given by

$$U(r) = ??. \tag{27}$$

I need to run this whole analysis to write down this part.

3 Numerical methods

In this section, different techniques will be presented to solve modal and non-modal stability problems for very large-scale dynamical systems. Such very large-scale systems typically arise from the spatial discretization of partial differential equations, e.g. the Navier-Stokes equations in fluid dynamics. Throughout this section,

the two-dimensional shear-driven cavity flow at various Reynolds numbers will serve as an example. The same configuration as [**?**] is considered. The dynamics of the flow are governed by

$$\begin{aligned} \frac{\partial \mathbf{U}}{\partial t} + (\mathbf{U}\cdot\nabla)\,\mathbf{U} &= -\nabla P + \frac{1}{Re}\nabla^2\mathbf{U} \\ \nabla\cdot\mathbf{U} &= 0, \end{aligned} \tag{28}$$

where $\mathbf{U}$ is the velocity field and P is the pressure field. Figure **??** depicts a typical vorticity snapshot obtained from direct numerical simulation at a supercritical Reynolds number.

Given a fixed point $\mathbf{U}_b$ of the Navier-Stokes equations (28), the dynamics of an infinitesimal perturbation $\mathbf{u}$ evolving on top of it are governed by

$$\begin{aligned} \frac{\partial \mathbf{u}}{\partial t} + (\mathbf{u}\cdot\nabla)\,\mathbf{U}_b + (\mathbf{U}_b\cdot\nabla)\,\mathbf{u} &= -\nabla p + \frac{1}{Re}\nabla^2\mathbf{u} \\ \nabla\cdot\mathbf{u} &= 0. \end{aligned} \tag{29}$$

Once projected onto a divergence-free vector space, Eq. (29) can be formally written as

$$\dot{\mathbf{u}} = \mathcal{A}\mathbf{u}, \tag{30}$$

where $\mathcal{A}$ is the linearized Navier-Stokes operator. After being discretized in space, $\mathcal{A}$ is a $n\times n$ matrix. For our example, the computational domain is discretized using ??? grid points, resulting in a total of $2\times$?? degrees of freedom. From a practical point of view, explicitly assembling the resulting matrix $\mathcal{A}$ would require approximately ?? Gb. Investigating the stability properties of this two-dimensional flow would thus not be possible on a simple laptop at the moment despite the simplicity of the case considered. It has to be noted however that, given an initial condition $\mathbf{u}_0$, the analytical solution to Eq. (30) reads

$$\mathbf{u}(T) = \exp(\mathcal{A}T)\,\mathbf{u}_0,$$

where $\mathcal{M} = \exp(\mathcal{A}T)$ is the exponential propagator introduced previously. Although assembling explicitly this matrix $\mathcal{M}$ is even harder than assembling $\mathcal{A}$, its application onto the vector $\mathbf{u}_0$ can easily be computed using a classical time-stepping code solving the linearized Navier-Stokes equations (29). Such a *time-stepper* approach has been popularized by [**?**]. In the rest of this section, the different algorithms proposed for fixed point computation, linear stability and non-modal stability analyses will heavily rely on this time-stepper strategy. The key point is that they require only minor modifications of an existing time-stepping code to be put into use.

3.1 Fixed points computation

The starting point when investigating a nonlinear dynamical system it to determine its fixed points. As discussed in §2.1, for a continuous-time dynamical system, such points are solution to

$$\boldsymbol{\mathcal{F}}(\mathbf{X}) = 0, \tag{31}$$

while one needs to solve

$$\mathbf{X} - \boldsymbol{\mathcal{G}}(\mathbf{X}) = 0 \tag{32}$$

for a discrete-time nonlinear dynamical system. In this section, three different fixed point solvers will be presented.

3.1.1 Selective Frequency Damping

Selective frequency damping is a fixed point computation technique proposed by Åkervik *et al.* [1] in 2006 and largely adapted from the original work of Pruett *et al.* [10, 11] on temporal approximate deconvolution models for large-eddy simulations. It has since become one of the standard approaches for fixed point computation in fluid dynamics due to its ease of implementation. Note that various implementations of the original selective frequency damping method have been proposed over the years [5, 6, 4]. Moreover, it has since been extented to compute steady states of the Reynolds-Averaged-Navier-Stokes (RANS) equations [12] as well as for the computation of unstable periodic orbits [14]. In the rest of this section, only the original formulation by Åkervik *et al.* [1] will be described.

Let us consider a fixed point $\mathbf{X}^*$ of the nonlinear system

$$\dot{\mathbf{X}} = \boldsymbol{\mathcal{F}}(\mathbf{X}).$$

If $\mathbf{X}^*$ is linearly unstable, then any initial condition $\mathbf{X}_0 \neq \mathbf{X}^*$ will quickly depart from $\mathbf{X}^*$. Using standard regularization techniques from control theory, the aim of selective frequency damping is thus to stabilize the linearly unstable fixed point $\mathbf{X}^*$. For that purpose, one can use proportional feedback control so that the forced system now reads

$$\dot{\mathbf{X}} = \boldsymbol{\mathcal{F}}(\mathbf{X}) - \chi(\mathbf{X} - \mathbf{Y}), \tag{33}$$

where χ is the control gain and $\mathbf{Y}$ the target solution. This target solution is obviously the fixed point one aims to stabilize, i.e. $\mathbf{Y} = \mathbf{X}^*$, which is unfortunately not known *a priori*. It has to be noted however that, for a large range of situations, the instability of the fixed point $\mathbf{X}^*$ will tend to give rise to unsteady dynamics. In such cases, the target solution $\mathbf{Y}$ is thus a modification of $\mathbf{X}$ with *reduced temporal fluctuations*, i.e. a temporally low-pass filtered solution. This filtered solution is defined as

$$\mathbf{Y}(t) = \mathcal{H}(t, \Delta) * \mathbf{X}(t - \tau) \tag{34}$$

where $\mathcal{H}$ is the convolution kernel of the applied causal low-pass filter and Δ the filter witdh. Using such definitions, the forced system (33) can thus be rewritten as

$$\dot{\mathbf{X}} = \boldsymbol{\mathcal{F}}(\mathbf{X}) - \chi(\mathcal{I} - \mathcal{H}) * \mathbf{X}. \tag{35}$$

As $\mathbf{X}$ tends to the fixed point $\mathbf{X}^*$, the low-pass filtered solution $\mathbf{Y}$ tends to $\mathbf{X}$. Once a steady state has been reached, one has

$$\mathbf{X} = \mathbf{Y} = \mathbf{X}^*,$$

i.e. the fixed point of the controlled system (35) is the same as that of our original system. Moreover, as the system approaches its fixed point, the amplitude of the proportional feedback control term vanishes.

Applying the low-pass filter in the time domain

As it is formulated, computing the low-pass filtered solution (34) requires the evaluation of the following convolution integral

$$\mathbf{Y}(t) = \int_{-\infty}^{t} \mathcal{H}(\tau - t, \Delta)\mathbf{X}(\tau)\mathrm{d}\tau. \tag{36}$$

Note that, to be admissible, the kernel $\mathcal{H}$ must be positive and properly normalized. Moreover, in the limit of vanishing filter width, it must approach the Dirac delta function. To the best of our knowledge, all implementations of the selective frequency damping thus relies on the exponential kernel

$$\mathcal{H}(\tau - t, \Delta) = \frac{1}{\Delta} \exp\left(\frac{\tau - t}{\Delta}\right). \tag{37}$$

The corresponding Laplace transform is given by

$$\hat{\mathcal{H}}(\omega, \Delta) = \frac{1}{1 + i\omega\Delta}. \tag{38}$$

The cutoff frequency of this filter is given by $\omega_c = 1/\Delta$. Figure 5 depicts the real part of $\hat{\mathcal{H}}$ as a function of the frequency ω for $\Delta = 1$. Naturally, this cutoff frequency needs to be tuned so that the frequency associated to the instability one aims to kill is quenched by the filter.

For real applications, evaluating the convolution integral (36) is impractical as it necessitates the storage of the complete time history of $\mathbf{X}$. Consequently, it is replaced by its differential form given by

$$\dot{\mathbf{Y}} = \frac{1}{\Delta}(\mathbf{X} - \mathbf{Y}) \tag{39}$$

which can be integrated in time using classical integration schemes, e.g. second-order backward Euler. Combining (39) and (33) finally yields to the following extended system

$$\begin{cases} \dot{\mathbf{X}} = \boldsymbol{\mathcal{F}}(\mathbf{X}) - \chi(\mathbf{X} - \mathbf{Y}) \\ \dot{\mathbf{Y}} = \dfrac{1}{\Delta}(\mathbf{X} - \mathbf{Y}). \end{cases} \tag{40}$$

Implementing (40) into an existing time-stepping code requires only minor modifications, hence making it an easy choice for fixed point computation. It must be emphasized however that, because it relies on a low-pass filtering procedure, this selective frequency damping method is unable to quench non-oscillating instabilities, e.g. instabilities arising due to a pitchfork bifurcation. This particular point is one of its major limitations.

3.1.2 Newton-Krylov methods

While we relied on the continuous time representation of our system in §3.1.1, we will now turn to its discrete-time counterpart in order to stay as close as possible to the actual time-stepper implementation of the algorithm to be describe. For that purpose, we will thus consider the following nonlinear system

$$\mathbf{X}_{k+1} = \boldsymbol{\mathcal{G}}(\mathbf{X}_k). \tag{41}$$

Our goal is thus to find a fixed point $\mathbf{X}$ of this problem. Newton-Raphson method is a natural choice, provided the dimension of $\mathbf{X}$ is not too large. For large-scale dynamical systems, one may turn to the class of Newton-Krylov methods instead. These encompasses a wide variety of different approaches, part of which have been reviewed in [8]. In the rest of this section, we will present a variant of the recursive projection method originally proposed by Shroff & Keller [15].

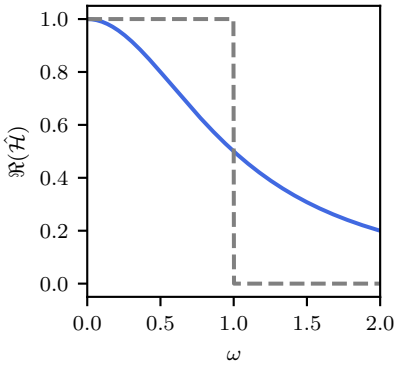

Fig. 5 Evolution of $\Re(\hat{\mathcal{H}})$ (—), i.e. the real part of the Laplace transform of the exponential filter, as a function of the frequency ω for $\Delta = 1$. The gray dashed line depicts the ideal spectral cutoff filter.

3.1.3 BoostConv

3.1.4 Comparison of the different approaches

3.2 Linear stability and eigenvalue computation

The aim of linear stability analysis is to determine whether a perturbation $\mathbf{x}$, governed by

$$\dot{\mathbf{x}} = \mathcal{A}\mathbf{x},$$

will grow or decay exponentially rapidly as $t \to \infty$. This asymptotic behavior is entirely governed by the eigenspectrum of the Jacobian matrix $\mathcal{A}$: if at least one of its eigenvalues has a positive (resp. negative) real part, the linear system considered is unstable (resp. stable), see §2.2 for more details.

It must emphasized that, within a time-stepper framework, one does not seek directly for the eigenpairs of the Jacobian matrix $\mathcal{A}$ of the continuous-time problem. Instead, the problem considered is recast in the discrete-time framework as

$$\mathbf{x}_{k+1} = \mathcal{M}\mathbf{x}_k, \tag{42}$$

where $\mathcal{M} = \exp(\mathcal{A}T)$ is the exponential propagator already introduced in §2.2, §2.3.1, and §3.1.2, and where T is the sampling period. The system is then linearly unstable if at least one eigenvalue μ of $\mathcal{M}$ lies outside the unit disk, i.e. $|\mu| > 1$.

As discussed previously, although one cannot explicitly assemble the exponential propagator $\mathcal{M}$, its action onto a given vector $\mathbf{x}_k$ simply amounts to march in time the linearized system from $t = kT$ to $t = (k+1)T$. This ability to evaluate relatively easily the matrix-vector product given by (42) allows us to use iterative solvers as to compute the eigenpairs of $\mathcal{M}$. The rest of this section is thus devoted to the presentation of two iterative eigenvalue solvers, namely the Arnoldi decomposition and the Krylov-Schur decomposition.

3.2.1 Arnoldi decomposition

Let us denote the following sequence of vectors

$$\mathcal{K}_m(\mathcal{M}, \mathbf{v}_0) = \left\{\mathbf{v}_0, \mathcal{M}\mathbf{v}_0, \cdots, \mathcal{M}^{m-1}\mathbf{v}_0\right\}. \tag{43}$$

Eq. (43) is known as a *Krylov sequence* eventually converging toward the eigenvector associated to the largest eigenvalue (in modulus) of $\mathcal{M}$ as $m \to \infty$. Generating this sequence to approximate the leading eigenpair of $\mathcal{M}$ is known as the *power iteration method*. Note that this simple method retains only the last vector of this sequence while discarding the information contained in the first $m-1$ vectors.

Contrary to the power iteration method, Arnoldi decomposition uses all of the information contained in the Krylov sequence (43) as to compute better estimates of the leading eigenvalues of $\mathcal{M}$. Readers can easily be convinced that the Krylov

sequence (43) obeys

$$\mathcal{M}\mathcal{K}_m \simeq \mathcal{K}_m\mathcal{C},$$

where $\mathcal{C}$ is a $m \times m$ companion matrix representing the low-dimensional projection of $\mathcal{M}$ onto the span of the Krylov sequence (43). As such, the eigenpairs of $\mathcal{C}$ approximate the leading eigenpairs of $\mathcal{M}$. It must be emphasized however that, as m increases, the last vectors in the Krylov sequence become almost parallel. Consequently, the companion matrix $\mathcal{C}$ becomes increasingly ill-conditioned. As to overcome the loss of information from the power iteration method and the increasingly ill-conditioned companion matrix decomposition, the Arnoldi method combines them with a Gram-Schmidt orthogonalization process. The basic Arnoldi iteration then reads

$$\mathcal{M}\mathcal{V}_m = \mathcal{V}_m\mathcal{H}_m + \mathbf{r}_m\mathbf{e}_m^T, \tag{44}$$

where $\mathcal{V}_m$ is an orthonormal set of vectors, $\mathcal{H}_m$ is a $m \times m$ upper Hessenberg matrix and $|\mathbf{r}_m\mathbf{e}_m^T|$ is the residual indicating how far $\mathcal{V}_m$ is from from an invariant subspace of $\mathcal{M}$. Because of its relatively small dimension, the eigenpairs $(\mu_H, \mathbf{y})$ of the Hessenberg matrix, also known as Ritz pairs, can be computed using direct eigensolvers, e.g. QZ decomposition. The Ritz pairs of $\mathcal{H}_m$ are related to the eigenpairs of $\mathcal{M}$ as follows

$$\begin{aligned} \mu_{\mathcal{M}} &\simeq \mu_{\mathcal{H}} \\ \hat{\mathbf{u}} &\simeq \mathcal{V}_m\mathbf{y}. \end{aligned} \tag{45}$$

A detailed presentation of the basic m-step Arnoldi factorization is given in algorithm (1) while figure 6 depicts its block-diagram representation to ease the understanding. As can be seen, Arnoldi decomposition is relatively simple to implement within an existing time-stepper code. One has to bear in mind however that this technique resembles some sophisticated signal processing. As a consequence, in order to capture (within a time-stepper framework) an eigenpair of the Jacobian matrix $\mathcal{A}$ characterized by a circular frequency ω, one has to obey the Nyquist criterion and needs at least four snapshots to appropriately discretize the associated period.

3.2.2 Krylov-Schur decomposition

Let us consider the m-step Arnoldi factorization

$$\mathcal{M}\mathcal{V}_m = \mathcal{V}_m\mathcal{H}_m + \beta\mathbf{v}_{m+1}\mathbf{e}_m^T \tag{46}$$

introduced in §3.2.1. As discussed previously, the Ritz pair $(\mu_H, \mathcal{V}_m\mathbf{y})$ of $\mathcal{H}_m$ provides a good approximation for the eigenpair $(\mu, \hat{\mathbf{u}})$ of the matrix $\mathcal{M}$. One limitation of the Arnoldi decomposition is however that the dimension m of the Krylov subspace necessary to converge the leading Ritz pairs is not known *a priori*. It might hence be relatively large, thus potentially causing some numerical and/or practical problems (e.g. storage of Krylov basis $\mathcal{V}_m$, forward instability of the Gram-Schmidt process involved in the Arnoldi decomposition, etc). Two different approaches have been proposed to overcome these limitations: the *Implicitly Restarted*

Algorithm 1 The *m*-step *Arnoldi* factorisation.

Require: $\boldsymbol{\mathcal{M}} \in \mathbb{R}^{n\times n}$, starting vector $\mathbf{v} \in \mathbb{R}^n$.
$\mathbf{v}_1 = \mathbf{v}/\|\mathbf{v}\|$;
$\mathbf{w} = \boldsymbol{\mathcal{M}}\mathbf{v}_1$;
$\alpha_1 = \mathbf{v}_1^T\mathbf{w}$;
$\mathbf{f}_1 \leftarrow \mathbf{w} - \alpha_1\mathbf{v}_1$;
$\boldsymbol{\mathcal{V}}_1 \leftarrow (\mathbf{v}_1)$;
$\boldsymbol{\mathcal{H}}_1 \leftarrow (\alpha_1)$;
for $j = 1, 2, \cdots, m-1$ **do**
  $\beta_j = \|\mathbf{f}_j\|$;
  $\mathbf{v}_{j+1} \leftarrow \mathbf{f}_j/\beta_j$;
  $\boldsymbol{\mathcal{V}}_{j+1} \leftarrow \left(\boldsymbol{\mathcal{V}}_j, \mathbf{v}_{j+1}\right)$;
  $\hat{\boldsymbol{\mathcal{H}}}_j \leftarrow \begin{pmatrix} \boldsymbol{\mathcal{H}}_j \\ \beta_j \mathbf{e}_j^T \end{pmatrix}$
  $\mathbf{w} \leftarrow \boldsymbol{\mathcal{M}}\mathbf{v}_{j+1}$;
  $\mathbf{h} \leftarrow \boldsymbol{\mathcal{V}}_{j+1}^T\mathbf{w}$;
  $\mathbf{f}_{j+1} \leftarrow \mathbf{w} - \boldsymbol{\mathcal{V}}_{j+1}\mathbf{h}$;
  $\boldsymbol{\mathcal{H}}_{j+1} \leftarrow (\hat{\boldsymbol{\mathcal{H}}}_j, \mathbf{h})$;
end for

Arnoldi Method introduced by Sorensen [16] in 1992 and the *Krylov-Schur decomposition* introduced by Stewart [17] in 2001. In the present work, the latter approach has been preferred because of its simplicity of implementation and its robustness.

The Krylov-Schur method is based on the generalization of the m-step Arnoldi factorization (46) to a *Krylov decomposition* of order *m*

$$\boldsymbol{\mathcal{M}}\boldsymbol{\mathcal{V}}_m = \boldsymbol{\mathcal{V}}_m\boldsymbol{\mathcal{B}}_m + \mathbf{v}_{m+1}\mathbf{b}_{m+1}^T \tag{47}$$

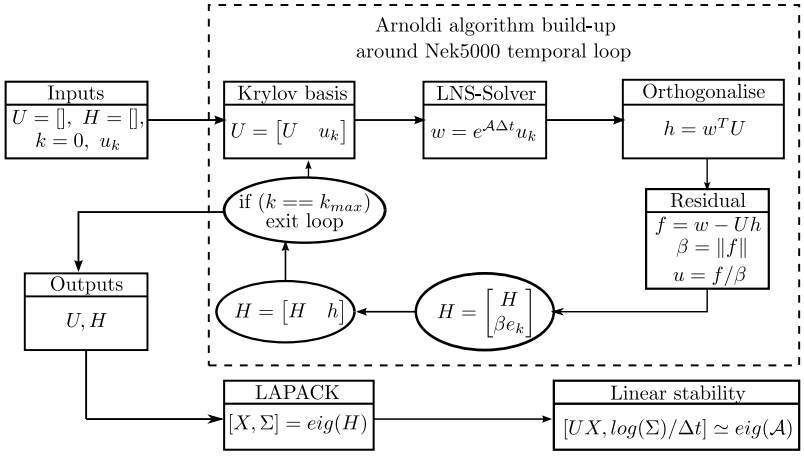

Fig. 6 Block-diagram representation of the basic *m*-step Arnoldi factorization. Note that, within a time-stepper framework, every matrix-vector product $\boldsymbol{\mathcal{M}}\mathbf{v}_i$ is evaluated by marching in time the linearized system considered.

in which the matrix $\mathcal{B}_m$ and the vector $\mathbf{b}_{m+1}$ have no restriction. The Arnoldi decomposition then appears as a special case of Krylov decomposition when $\mathcal{B}_m$ is restricted to be in upper Hessenberg form and $\mathbf{b}_{m+1} = \mathbf{e}_m$. Another special case is the *Krylov-Schur* decomposition in which the matrix $\mathcal{B}_m$ is in real Schur form (i.e. quasi-triangular form with its eigenvalues in the 1×1 or 2×2 diagonal blocks). It has been shown by Stewart [17] that Krylov and Arnoldi decompositions are equivalent (i.e. they have the same Ritz approximations). Moreover, by means of orthogonal similarity transformations, any Krylov decomposition can be transformed into an equivalent Krylov-Schur decomposition. The core of the Krylov-Schur method is thus based on a two-steps procedure: (*i*) an expansion step performed using a m-step Arnoldi factorization, and (*ii*) a contraction step to a Krylov-Schur decomposition of order p retaining only the most useful spectral information from the initial m-step Arnoldi decomposition. Given an initial unit-norm vector $\mathbf{v}_1$, a subroutine to compute the matrix-vector product $\mathcal{M}\mathbf{v}_i$, and the desired dimension m of the Krylov subspace, the Krylov-Schur method can be summarized as follows:

1. Construct an initial Krylov decomposition of order m using for instance the m-step Arnoldi factorization (46).
2. Check for the convergence of the Ritz eigenpairs. If a sufficient number has converged, then stop. Otherwise, proceed to step 3.
3. Compute the real Schur decomposition $\mathcal{B}_m = \mathcal{Q}\mathcal{S}_m\mathcal{Q}^T$ such that the matrix $\mathcal{S}_m$ is in real Schur form and $\mathcal{Q}$ is the associated matrix of Schur vectors. It is assumed furthermore that the Ritz values on the diagonal blocks of $\mathcal{S}_m$ have been sorted such that the p "wanted" Ritz values are in the upper-left corner of $\mathcal{S}_m$, while the $m-p$ "unwanted" ones are in the lower-right corner. At this point, we have the following re-ordered Krylov-Schur decomposition

$$\mathcal{M}\tilde{\mathcal{V}}_m = \tilde{\mathcal{V}}_m \begin{bmatrix} \mathcal{S}_{11} & \mathcal{S}_{12} \\ \mathbf{0} & \mathcal{S}_{22} \end{bmatrix} + \mathbf{v}_{m+1} \begin{bmatrix} \mathbf{b}_1^T & \mathbf{b}_2^T \end{bmatrix} \tag{48}$$

   with $\tilde{\mathcal{V}}_m = \mathcal{V}_m\mathcal{Q}$ being the re-ordered Krylov basis, $\mathcal{S}_{11}$ the subset of the Schur matrix containing the p "wanted" Ritz values, $\mathcal{S}_{22}$ the subset containing the $m-p$ "unwanted" ones, and $\begin{bmatrix} \mathbf{b}_1^T & \mathbf{b}_2^T \end{bmatrix} = \mathbf{b}^T\mathcal{Q}$.
4. Truncate the Krylov-Schur decomposition (48) of order m to a Krylov decomposition of order p,

$$\mathcal{M}\tilde{\mathcal{V}}_p = \tilde{\mathcal{V}}_p\mathcal{S}_{11} + \tilde{\mathbf{v}}_{p+1}\mathbf{b}_1^T \tag{49}$$

   with $\tilde{\mathcal{V}}_p$ equal to the first p columns of $\tilde{\mathcal{V}}_m$ and $\tilde{\mathbf{v}}_{p+1} = \mathbf{v}_{m+1}$.
5. Extend again to a Krylov decomposition of order m using a variation of the procedure used in the first step: the procedure is re-initialized with the starting vector $\mathbf{v}_{p+1}$ but all the vectors in $\tilde{\mathcal{V}}_p$ are taken into account in the orthogonalization step.
6. Check the convergence of the Ritz values. If not enough Ritz values have converged, restart from step 3.

This algorithm has two critical steps. The first one is the choice of the "wanted" Ritz values in the re-ordering of the Schur decomposition in step 2. Since we are only interested in the leading eigenvalues of the linearized Navier-Stokes operator,

all the Ritz pairs being classified as "wanted" must satisfy $|\mu_w| \geq 1-\delta$ (with $\delta = 0.05-0.1$ usually). Regarding the criterion assessing the convergence of a given Ritz pair, starting from the Krylov decomposition (46), one can write

$$\|\boldsymbol{\mathcal{M}}\boldsymbol{\mathcal{V}}_m\mathbf{y} - \boldsymbol{\mathcal{V}}_m\boldsymbol{\mathcal{B}}_m\mathbf{y}\| = \|\boldsymbol{\mathcal{M}}\boldsymbol{\mathcal{V}}_m\mathbf{y} - \mu_{\mathbf{B}}\boldsymbol{\mathcal{V}}_m\mathbf{y}\| = \left|\beta\mathbf{e}_m^T\mathbf{y}\right| \tag{50}$$

with $(\mu_{\mathbf{B}}, \mathbf{y})$ a given eigenpair of the matrix $\boldsymbol{\mathcal{B}}_m$. If the right hand side $\left|\beta\mathbf{e}_m^T\mathbf{y}\right|$ is smaller than a given tolerance, then the Ritz pair $(\mu_{\mathbf{B}}, \boldsymbol{\mathcal{V}}_m\mathbf{y})$ provides a good approximation to the eigenpair $(\mu, \hat{\mathbf{u}})$ of the original matrix $\boldsymbol{\mathcal{M}}$. A Ritz value is generally considered as being converged if the associated residual $\left|\beta\mathbf{e}_m^T\mathbf{y}\right| \leq 10^{-6}$.

3.2.3 Comparison of the two approaches

3.3 Non-modal stability and singular value decomposition

3.3.1 Optimal perturbation analysis

3.3.2 Resolvent analysis

4 Application to fluid dynamics

5 Conclusions and perspectives

References

1. E Åkervik, L Brandt, D S Henningson, J Hœpffner, O Marxen, and P Schlatter. Steady solutions of the navier-stokes equations by selective frequency damping. *Physics of fluids*, 18(6):068102, 2006.
2. S Boyd and L Vandenberghe. *Convex optimization*. Cambridge university press, 2004.
3. L Brandt. The lift-up effect: The linear mechanism behind transition and turbulence in shear flows. *European Journal of Mechanics-B/Fluids*, 47:80–96, 2014.
4. Guilherme Cunha, Pierre-Yves Passaggia, and Marc Lazareff. Optimization of the selective frequency damping parameters using model reduction. *Physics of Fluids*, 27(9):094103, 2015.
5. Bastien E. Jordi, Colin J. Cotter, and Spencer J. Sherwin. Encapsulated formulation of the selective frequency damping method. *Physics of Fluids*, 26(3):034101, 2014.
6. Bastien E. Jordi, Colin J. Cotter, and Spencer J. Sherwin. An adaptive selective frequency damping method. *Physics of Fluids*, 27(9):094104, 2015.
7. R R Kerswell, C C T Pringle, and A P Willis. An optimization approach for analysing nonlinear stability with transition to turbulence in fluids as an exemplar. *Reports on Progress in Physics*, 77(8):085901, 2014.
8. D A Knoll and D E Keyes. Jacobian-free newton–krylov methods: a survey of approaches and applications. *Journal of Computational Physics*, 193(2):357–397, 2004.
9. M T Landahl. A note on an algebraic instability of inviscid parallel shear flows. *Journal of Fluid Mechanics*, 98(2):243–251, 1980.
10. C D Pruett, T B Gatski, C E Grosch, and W D Thacker. The temporally filtered navier–stokes equations: properties of the residual stress. *Physics of Fluids*, 15(8):2127–2140, 2003.

11. C D Pruett, B C Thomas, C E Grosch, and T B Gatski. A temporal approximate deconvolution model for large-eddy simulation. *Physics of Fluids*, 18(2):028104, 2006.
12. F. Richez, M. Leguille, and O. Marquet. Selective frequency damping method for steady rans solutions of turbulent separated flows around an airfoil at stall. *Computers & Fluids*, 132(Supplement C):51 – 61, 2016.
13. P J Schmid and L Brandt. Analysis of fluid systems: Stability, receptivity, sensitivity. Lecture notes from the FLOW-NORDITA summer school on advanced instability methods for complex flows, Stockholm, Sweden, 2013. *Applied Mechanics Reviews*, 66(2):024803, 2014.
14. Léopold Shaabani-Ardali, Denis Sipp, and Lutz Lesshafft. Time-delayed feedback technique for suppressing instabilities in time-periodic flow. *Physical Review Fluids*, 2(11):113904, 2017.
15. G M Shroff and H B Keller. Stabilization of unstable procedures: the recursive projection method. *SIAM Journal on numerical analysis*, 30(4):1099–1120, 1993.
16. D. C. Sorensen. Implicit application of polynomial filters in a k-step Arnoldi method. *SIAM J. Matrix Anal. Appl.*, 13:357–385, 1992.
17. G. W. Stewart. A Krylov-Schur algorithm for large eigenproblems. *SIAM J. Matrix Anal. Appl.*, 23:601–614, 2001.